Available online at www.sciencedirect.com

ScienceDirect

Advances in Space Research xxx (2019) xxx–xxx

ADVANCES IN SPACE RESEARCH (a COSPAR publication)

www.elsevier.com/locate/asr

Neural network aided fast pointing information determination approach for occultation payloads from in-flight measurements: Algorithm design and assessment ☆

Songyan Zhu [a,b], Xiaoying Li [b,*,1], Jian Xu [c], Tianhai Cheng [b], Xingying Zhang [d] Hongmei Wang [b,e], Yapeng Wang [b,e], Jing Miao [b,e]

[a] China Centre for Resources Satellite Data and Application, Beijing 100830, China
[b] State Key Laboratory of Remote Sensing Science, Institute of Remote Sensing and Digital Earth, Chinese Academy of Sciences, Beijing 100101, China
[c] Remote Sensing Technology Institute, German Aerospace Center (DLR), Oberpfaffenhofen, Germany
[d] National Satellite Meteorological Center, China Meteorological Administration, Beijing 100081, China
[e] School of Electronic, Electrical, and Communication Engineering, University of Chinese Academy of Sciences, Beijing 100049, China

Received 19 June 2018; received in revised form 10 December 2018; accepted 27 January 2019

Abstract

Pointing information is decisive to solving precise profile retrieval issues from occultation measurements. Research regarding stratospheric O_3 hole in Antarctic and surface O_3 pollution would significantly benefit from massive occultation measurements. A neural network aided pointing information determination approach, in terms of tangent heights, is proposed to address issues requiring fast and easy-to-use determined tangent heights. The geometrical triangular iteration (GTI) algorithm in this work is based on N_2 absorption microwindows, and several treatments (e.g., tangential stride generator and triangular-net optimization) are adopted. In addition, LSTM is employed to reduce time consumption and increase accuracy. Atmospheric Chemistry Experiment-Fourier Transform Spectrometer (ACE-FTS) in-flight measurements are used to assess this approach. The comparison between the proposed algorithm and eight official products indicates a promising performance. Correlation coefficient for each orbit is greater than 0.99. The processing time is about 16.6 min per orbit with an average cost of ~0.06. The introduction of LSTM technique demonstrates an approximate 28.49% better result, with less computation time. It costed less than 30 s to determine eight orbit tangent heights. In general, although minor issues remain, this LSTM-aided GTI algorithm is applicable in industry.

Keywords: Occultation observation; Pointing information; N_2 absorption; Tangential strides; Triangular iteration; LSTM

1. Introduction

Stratospheric O_3 is crucial to radiative coercion and ultraviolet radiation fluxes while its surficial counterpart is a primary pollutant in worldwide populace intensive cities, e.g. Los Angeles and Beijing (Ofipcc, 2013; Zhou et al., 2017; Chung et al., 2014; Sandy et al., 2004). Comprehensive understanding of its profile can be instructive for surface O_3 induced pollution monitoring. Remote sensing technique allows labor-saving O_3 profile observations

☆ This template can be used for all publications in Advances in Space Research.

* Corresponding author.
E-mail addresses: soonyenju@outlook.com (S. Zhu), lixy01@radi.ac.cn (X. Li), jian.xu@DLR.de (J. Xu), chength@radi.ac.cn (T. Cheng), zxy@cma.gov.cn (X. Zhang), wwhongmei@126.com (H. Wang), wangyp@radi.ac.cn (Y. Wang), miaojing16@mails.ucas.ac.cn (J. Miao).
[1] Assitant professor, major in atmospheric detection and occultation observation.

https://doi.org/10.1016/j.asr.2019.01.041
0273-1177/

in global scale. Various satellite-based occultation datasets offer opportunities for researchers to investigate the Antarctic ozone hole and analyze the near ground pollution sources (Zhu et al., 2018; Castellanos et al., 2015; Suleiman et al., 2013; George et al., 2009; Voulgarakis et al., 2011; Harrison et al., 2014). It is challenging to obtain profile information with high vertical-resolutions via ultraviolet payloads (Wang et al., 2017; Jethva et al., 2011). One remaining issue in occultation payloads, such as Atmospheric Chemistry Experiment-Fourier transform spectrometer (ACE-FTS) and Stratospheric Aerosol and Gas Experiment (SAGE) II, is the determination of pointing information (LI et al., 2013; Urban, 2014; Steck et al., 2008; Cortesi et al., 2016). The pointing information is the vertical heights of tangent points of line-of-sight and atmosphere. The SCISAT-1 is a Canadian scientific experimental satellite mission. ACE-FTS is one payload onboard SCISAT-1 (Sioris et al., 2010; Manney et al., 2008). It and another sensor were designed for improving the understanding of atmospheric chemistry, climate change and aerosol/cloud extinction. Except for ACE-FTS, many other occultation payloads have been out of operation (Bernath, 2003). Under this circumstance, the Atmospheric Infrared Ultraspectral Sounder (AIUS) onboard Chinese satellite Gaofen-5 (GF5) was launched on May 9th, 2018 to satisfy the urgent needs of occultation measurements. The pointing information, also known as tangent heights, is decisive to profile inversion accuracy (Hendrick et al., 2007; Foucher et al., 2008).

Major limitations of present tangent height determination include CO_2 mixing-ratio assumption, interdependency of tangent heights with temperature and algorithm complexity which might introduce local uncertainties. Current approach retrieves tangent height determination synchronously when pressure/temperature (hereafter as p/T) are analyzed (Foucher et al., 2007; Boone et al., 2005). This treatment considering pointing information as a parameter is dependent on the CO_2 lines pre-selection which is reported questionable in many cases. For instance, CO_2 mixing ratio variation accounts for a minor error up to ~10 while this method is way more problematic in troposphere due to its weak lines (Foucher et al., 2007). Additionally, occultation payloads operate at sunrise and sunset, the value difference, i.e. sunrise-sunset difference (SSD) is up to comparatively large. As reported, an approximate 10% SSD was observed for SAGE II in stratosphere between 33 and 35 km, but for ACE-FTS, the observed SSD has not been reported in detail (Terao and Logan, 2005). Part of SSD is attributed to the instrumental and retrieval bias, and this factor might be close to the accuracy of tangent heights. A fast, easy-to-use determination approach of tangent height, therefore, is the imperative prerequisite for subsequent profiles retrievals and is urgently in need. In previous studies, N_2 collision induced absorption continuum near 2500 cm^{-1} was adopted to achieve a satisfactory tangent height N_2 retrieval (Foucher et al., 2007). Admittedly, this approach demonstrates a superior performance in laboratory environment with the employment of multiple customized treatments as reported (Boone et al., 2005). However, industry application requires a faster and more easy-to-use method. Extensive reproduction of this algorithm is unfortunately limited in industry environment, because the details of this tangent height determination algorithm cannot be fully revealed.

The official ACE-FTS algorithm is not for public access, therefore the study from scratch for ACE-FTS tangent height correction could be a helpful paradigm for subsequent similar occultation payloads, e.g. GF5-AIUS. An easy-to-use geometrical algorithm on pointing-information determination is proposed in this study for occultation payloads in operational environment. Details on the design and development of this algorithm (i.e., geometrical triangular iteration (GTI) algorithm) will be described, whilst the results of relative experiments on ACE-FTS Level-1 data will be demonstrated and discussed. Additionally, this algorithm adopts techniques (e.g., triangular-net, multicore computation) to reduce time consumption and employs neural network model for fine-tuning. All information will be presented and discussed.

2. Experiment data

From late 1970s, occultation sensors have been in service include the Halogen Occultation Experiment (HALOE), Stratospheric Aerosol and Gas Experiment (SAGE) series and Fourier Transform Spectrometer onboard SCISAT-1 of the Atmospheric Chemistry Experiment (ACE-FTS). Except for ACE-FTS, HALOE and SAGE III were terminated in 2005 and 2006, respectively. In addition, SCanning Imaging Absorption SpectroMeter for Atmospheric CHartographY (SCIAMACHY) onboard Envisat is regarded as one of the most important instruments that can operate in nadir, limb, occultation modes during the past decade. It has provided valuable measurements since 2002 but the Envisat mission was terminated in 2012. Considering the urgent demands for occultation measurements, the Atmospheric Infrared Ultraspectral Sounder (AIUS) onboard Chinese satellite Gaofen-5 (GF5) was launched on May 9^{th}, 2018. The AIUS is designed and developed with similar instrument characteristics to ACE-FTS. The SCISAT-1 is a Canadian scientific experimental satellite mission. It was launched in Aug. 2003, covering 85°N to 85°S, in low circular orbit with the inclination of 74° to provide high latitude occultation observations. The main purposes of ACE are to understand chemical and dynamical processes that control the distribution of O_3 in stratosphere and upper troposphere; to explore the relationship between atmospheric chemistry and climate change; to study the effects of biomass burning in the free troposphere; and to measure aerosols and clouds to reduce uncertainties in their effects on the global energy balance (Sioris et al., 2010; Manney et al., 2008). ACE carries two important payloads, a high resolution (0.02 cm^{-1})

Please cite this article as: S. Zhu, X. Li, J. Xu et al., Neural network aided fast pointing information determination approach for occultation payloads from in-flight measurements: Algorithm design and assessment, Advances in Space Research, https://doi.org/10.1016/j.asr.2019.01.041

Fourier-transform spectrometer (ACE-FTS) and Measurement of Aerosol Extinction in the Stratosphere and Troposphere Retrieved by Occultation (MAESTRO), which is designed in 285 nm-1030 nm with a vertical resolution about 1–2 km, providing measurements of O_3, NO_2 and aerosol/cloud extinction (Bernath, 2003).

ACE-FTS is a Michelson interferometer operating from 750 cm^{-1} to 4400 cm^{-1} in mid-IR (Kerzenmacher et al., 2008). It features high resolution, wide spectral coverage. Its orbital circulation is 98 min and it obtains 15 occultations per day. ACE-FTS provides the profile information for p/T mainly in 10–100 km. Besides, its inversion procedures cover volume mixing ratios (VMRs) for dozens of atmospheric components (e.g., H_2O, O_3, N_2O, CO, CH_4, NO, NO_2 et al.). About profile performance, very good absolute concentration determination is limited by the high-resolution transmission molecular absorption database (HITRAN) issues and calibration cannot change over time (Rothman et al., 2013). The vertical resolution is about 3 km and vertical sampling is about 1 km. In the lower atmosphere, the profile is mainly limited by cloud and spectral saturation; while in upper atmosphere, the profile is limited by sensitivity. As reported, ACE-FTS has shown remarkably stable operation on orbit, and it exceeds designed operational lifetime with no significant degradation or impact on the reliability (Dutil and Poulin, 2002). Table 1 provides the obtained date and coordinates of eight ACE-FTS Level-1 orbit transmittance data adopted in this study. In addition, the corresponding official Level-2 tangent-height products are used to compare our retrieval results of the experiment. Terms in this study are introduced as follows: (1) pointing information can be measured in terms of tangent heights, and the tangent height indicates the vertical height of tangent point of LOS (line of sight) and the atmosphere; (2) the Level-1 tangent height is uncorrected tangent height, it is usually directly derived from satellite ephemeris and observation geometry; (3) the Level-2 tangent height describes corrected tangent height adopting approaches like GTI algorithm and ACE-FTS official algorithm. Level-2 tangent height includes ACE-FTS official Level-2 tangent height products and tangent height determined by GTI. Here, if no special explanation, the Level-2 tangent height denotes the official ACE-FTS Level-2 products by default. (In fact, the official corrected tangent heights released to users are tagged as "Level-1" products. The conventional term "Level-2" is used instead in this study to disambiguate, the same below.).

Table 1
Obtained date and geolocation center coordinates of eight ACE-FTS orbits used to conduct the experiment.

Scene ID	Date	Longitude	Latitude
38154	Sept. 13, 2010	−73°	63°
43544	Sept. 14, 2011	75°	63°
43611	Sept. 18, 2011	−119°	70°
40993	Mar. 25, 2015	87°	−78°
48359	Aug. 5, 2015	−72°	−66°
39926	Jan. 11, 2011	131°	−68°
41738	May 14, 2011	16°	−65°
47073	May 10, 2012	59°	−67°

3. Theoretical basis

3.1. Sensitivity analysis

Fig. 1 offers the ACE-FTS transmittance in the wavenumber range 2490–2520 cm^{-1}. This range is adopted commonly as the tangent height correction window under the support of N_2 continuum absorption. In this range, transmittance varies little among orbits, and the shapes of absorption line are very similar, although the fitting slants of orbital transmittance show slightly obvious. Strongly absorbing regions are wavenumbers around 2495 cm^{-1} and region 2510–2520 cm^{-1}. The similarity of vertically averaged transmittance implies that the sensitivity method for ACE-FTS like occultation instrument might be applicable with robustness.

Additionally, in terms of transmittance for different height levels, Fig. 2 provides necessary information to evaluate the feasibility of correction algorithm. The obvious pattern shown in Fig. 2 indicates that the correction algorithm is supposed to be layer dynamic, that is flexible treatments for tangent heights in different height ranges. In virtue of figure above to assess transmittance variations, clearly in heights above 60 km the transmittance is almost stable near to 1. Transmittance decreases almost linearly along heights lower than 20 km. The steep decline slows down in height of 20–40 km which makes transmittance variation in this range stays a transition state. Accordingly, correction algorithm is designed on basis of tangent heights fall into three classes: lower atmosphere (<20 km), middle atmosphere (20–40 km) and upper atmosphere (>40 km).

According to the HITRAN database, Table 2 gives the N_2 absorption coefficients in spectral region (2490 cm^{-1} to 2520 cm^{-1}) that is adopted in this study. Despite of the relatively weak absorption, five absorption lines can be obtained in this spectral region. For N_2 absorption coefficients in this spectral region, relatively stronger absorption is found in smaller wavenumbers and vice versa; e.g., the absorption in 2491.77 cm^{-1} is about 6.17 times of absorption in 2512.92 cm^{-1}. The average absorption strength in this region is about 1.29×10^{-29} cm^{-1}, and it is scarcely deniable that the average strength is relatively weak. To satisfy the requirements of sample size and achieve a reliable correction accuracy, microwindows that include ~100 wavenumbers with a spectral resolution of 0.02 cm^{-1} are initialized.

Because other species might have stronger absorption in this region (i.e., initial microwindows) and consequently cause uncertainties, the sensitivity analysis mentioned before is conducted by means of taking potential gaseous components (e.g., CO, CH_4 and NO) into consideration.

Please cite this article as: S. Zhu, X. Li, J. Xu et al., Neural network aided fast pointing information determination approach for occultation payloads from in-flight measurements: Algorithm design and assessment, Advances in Space Research, https://doi.org/10.1016/j.asr.2019.01.041

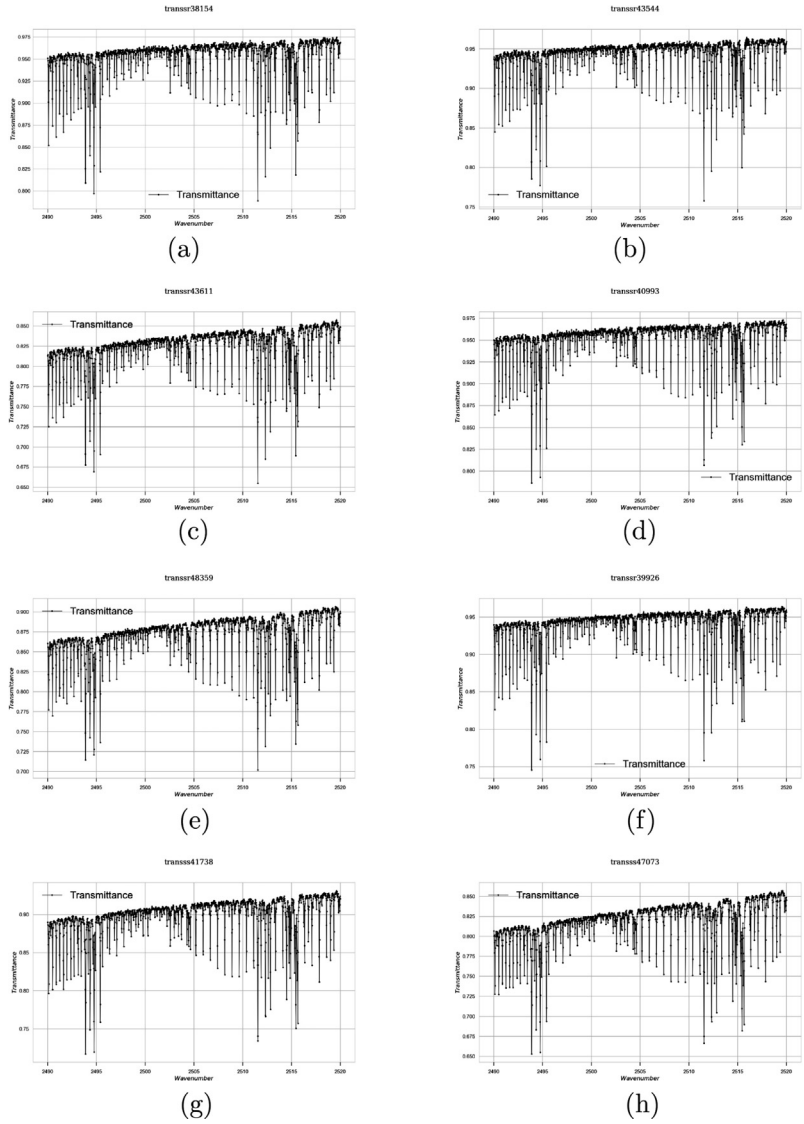

Fig. 1. Vertical average transmittance for 8 experiment ACE-FTS orbits. Each subplot shows corresponding orbital data as indicated by title.

The CH_4, H_2O and O_3, by comparison, are relatively more influential on N_2 absorption in multiple layers in initial microwindows. Fig. 3 gives the multiple layer averaged differential transmittance results of N_2 (a), CH_4 (b), H_2O (c), O_3 (d), respectively. While other compounds are insensitive in this region, the results of three disturbing absorbers are sensitive in diverse level and exhibit different distributions. H_2O absorption is less sensitive in this region with the smallest averaged differential transmittance. Therefore, the interference from H_2O can be neglected in this study. The differential transmittance of O_3 is at the same order of magnitude with N_2 and comparatively many absorption lines are observed in the figure; thereby the influence of O_3 is taken into consideration in the refinement of microwindows. Compared with other absorbers, CH_4 is the most sensitive and possibly imposes the most impacts on N_2 with three major absorptive peaks. Additionally, the average differential transmittance of CH_4 is about two orders of magnitude larger than N_2. Accordingly, the CH_4 and O_3 absorptive regions are eliminated from the initial microwindows while the H_2O absorption which contributes a small fraction is ignored.

3.2. GTI algoritm design

Because of the operational environment requirements, a fast, easy-to-use geometrical computation algorithm (i.e., the GTI algorithm) for tangent height correction is proposed in virtue of N_2 continuum absorption and the triangular iteration with tangential strides technique.

The flowchart describing the process for tangent heights correction is presented in Fig. 4, which can be summarized as two parts as follows: (1) the determination of tangent heights in the middle and upper atmosphere; (2) the correction for tangent heights in the lower atmosphere. The input data are the preprocessed Level-1 tangent heights and corresponding transmittances; while the output data are the corrected tangent heights. The cost function is defined as

Please cite this article as: S. Zhu, X. Li, J. Xu et al., Neural network aided fast pointing information determination approach for occultation payloads from in-flight measurements: Algorithm design and assessment, Advances in Space Research, https://doi.org/10.1016/j.asr.2019.01.041

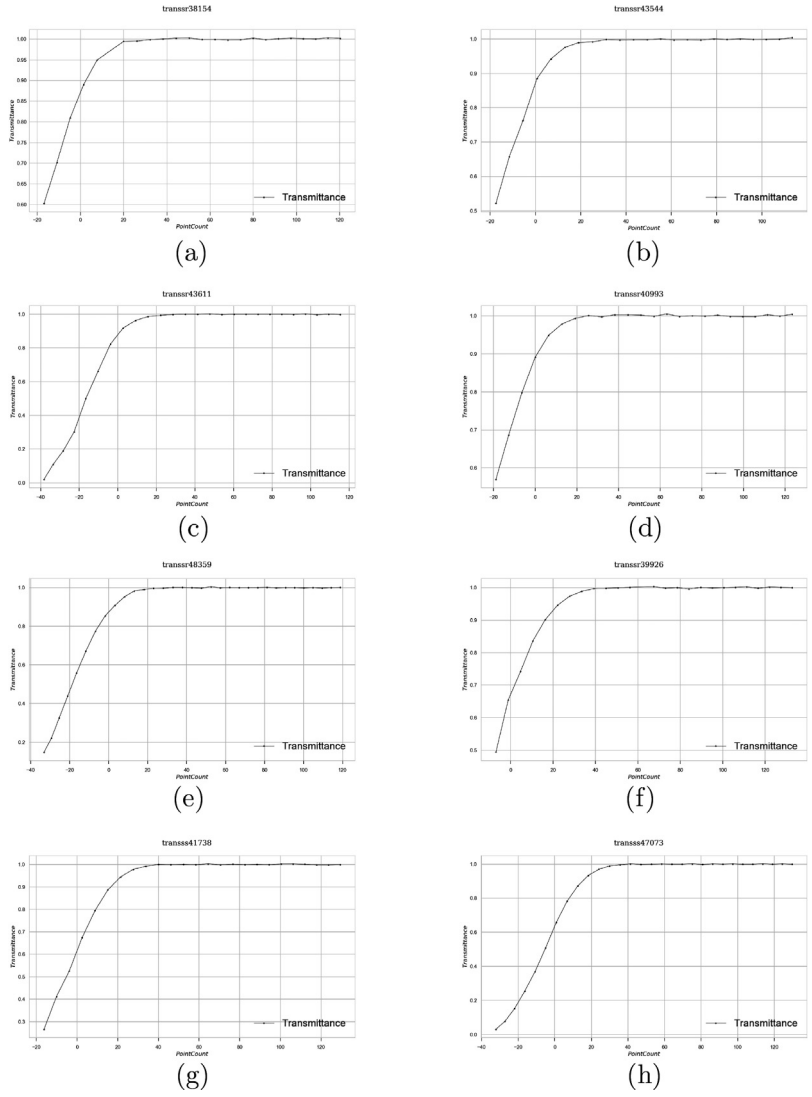

Fig. 2. Spectral averaged transmittance in Level-1 ACE-FTS tangent heights for each orbit, and the orbit number is represented by titles of subplots.

Table 2
N_2 absorption coefficients in the studied spectral region (2490 cm^{-1} to 2520 cm^{-1}).

Wavenumber (cm^{-1})	Absorption coefficient ($\times 10^{-29}$ cm^{-1})
2491.77	2.90
2498.86	1.02
2505.91	1.41
2512.92	0.47
2519.89	0.63

the quadratic sum loss between observed and simulated transmittances; and the convergence reaches if the quadratic sum loss is less than 0.01 or, concerning of the time requirement in operational processing system, the iteration count reaches the predefined iteration number (e.g., 10 times here).

According to previous studies, the feasibility of N_2 continuum near 4.0 μm was investigated and it has been applied in tangent height correction (Foucher et al., 2008; Lafferty et al., 1996). As suggested, the N_2 absorptive spectral region (i.e., 2490 cm^{-1} to 2520 cm^{-1} including 1500 wavenumbers) is adopted. To eliminate interfering absorbers, HITRAN (v 2012) spectroscopic parameters are used to calculate the difference between simulated spectra by increasing VMR of each species and corresponding original simulations separately.

Forward model is one theoretical basis and indispensable tool in the implementation of tangent height correction. The Atmospheric Radiative Transfer Simulator (ARTS) is an open-source model for the simulation of atmospheric radiative transfer from microwave to infrared spectral range (i.e., millimeter and submillimeter) (Buehler et al., 2005). ARTS development is based on the principle of providing a widely applicable model accommodating simulations for different viewing geometries that are defined by Line-of-Sight (LOS) and sensors; thereby the modularity, extendibility and generality were highly taken into consideration. The current ARTS version is v 2.0

Please cite this article as: S. Zhu, X. Li, J. Xu et al., Neural network aided fast pointing information determination approach for occultation payloads from in-flight measurements: Algorithm design and assessment, Advances in Space Research, https://doi.org/10.1016/j.asr.2019.01.041

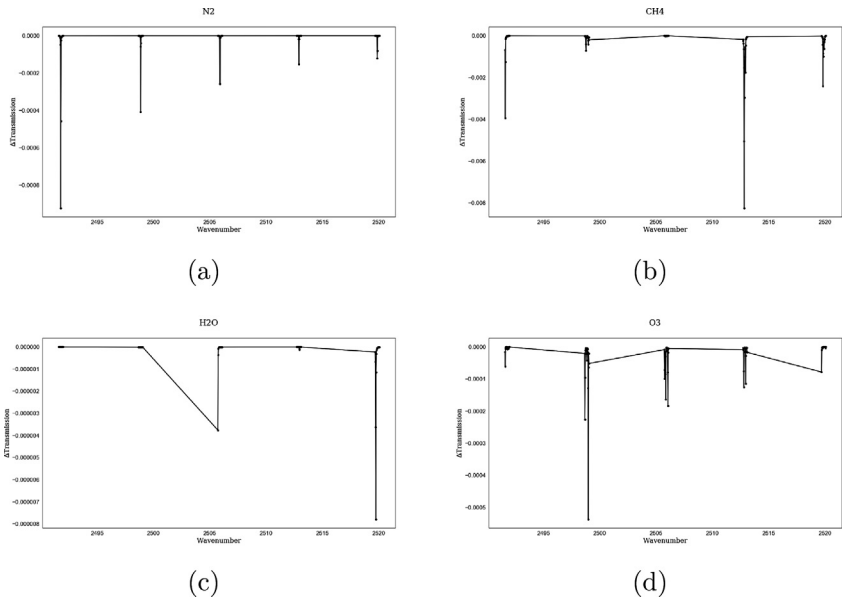

Fig. 3. Differential transmittance based on HITRAN profiles of N_2 (a) and three other gaseous components might be influential, that is CH_4 (b), H_2O (c), O_3 (d), respectively.

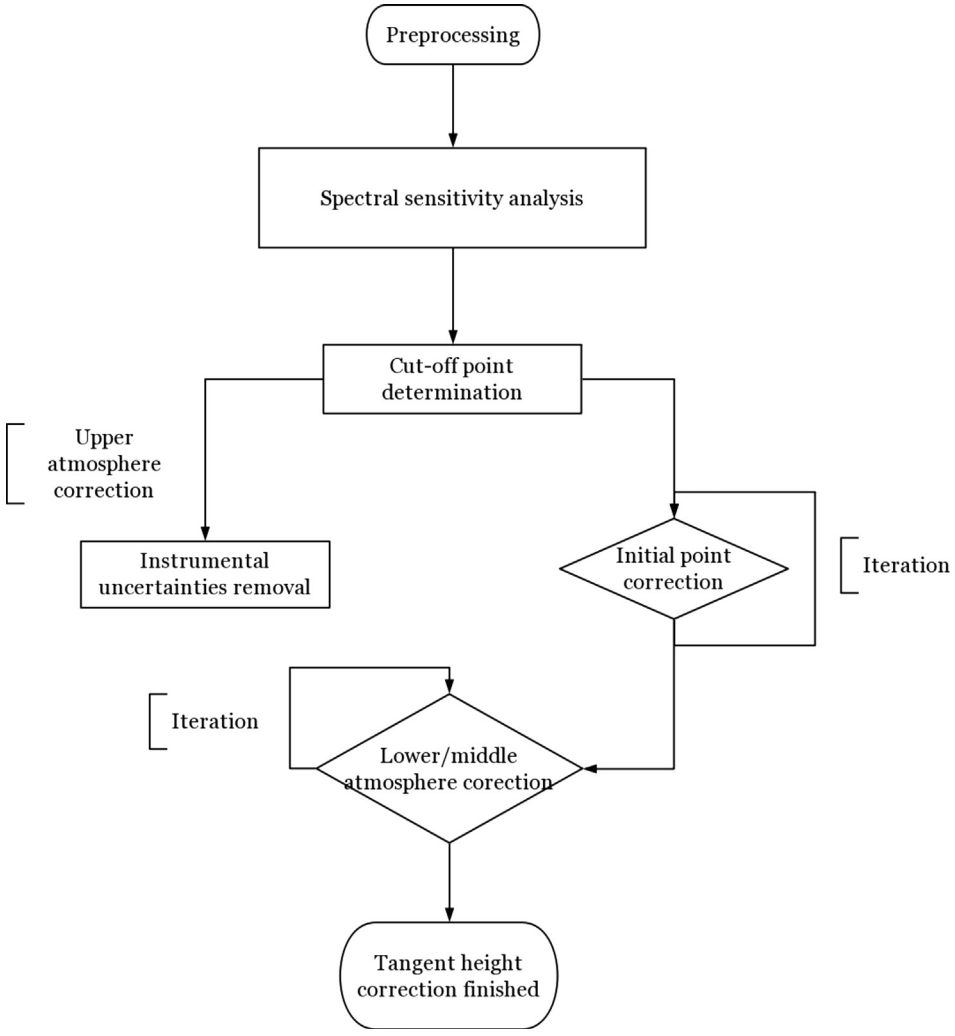

Fig. 4. Flowchart of GTI tangent heights correction.

Please cite this article as: S. Zhu, X. Li, J. Xu et al., Neural network aided fast pointing information determination approach for occultation payloads from in-flight measurements: Algorithm design and assessment, Advances in Space Research, https://doi.org/10.1016/j.asr.2019.01.041

which combines multiple features; for example, it adopts state-of-art absorption models and there are no intrinsic limitations for viewing geometry (i.e., nadir, limb and occultation observation geometries and other arbitrary observation directories) (Eriksson et al., 2011; Xiaoying et al., 2015; Höpfner and Emde, 2005).

Instrumental and systematic uncertainties can be influential in tangent height correction and subsequent retrievals. Above upper troposphere, gaseous components only contribute a relatively small fraction in satellite observing transmittances. Accordingly, impacts imposed on ACE-FTS transmittances above ~40 km can be attributed to systematic uncertainties. In lower atmosphere (i.e., lower than 20 km) and middle atmosphere (i.e., 20–40 km), the satellite measurements are influenced by both systematic uncertainties and geophysical/atmospheric contributors (e.g., ground surface refraction, the Earth curvature and gases absorption/emission). Consequently, whilst being linear in upper atmosphere, tangent height series in lower/middle atmosphere is quadratic, and the cut-off point between upper atmosphere and in lower/middle can be determined according to the second order difference.

The correction for tangent heights in the lower and middle atmosphere includes two critical parts: (1) first-guess for initial tangent point (i.e., the first point in tangent height series) and its determination with tangential iterative strides; (2) constructing possible tangent height pool and conducting optimization for tangent height series by employing triangular iteration.

Fig. 5 shows the basic structure of triangular-net for tangent height series in lower/middle atmosphere. Initial point (i.e., the lowest/first tangent point), moving point and cut-off point are dominant in the construction for iterative triangular-net. Moving point is defined as the tangent point with the largest curvature in series, that is, the tangent point imposes the most impacts on the shape of triangular-net. Ditto, the second order difference is a good method for position determination of moving point in tangent height series.

The exact position for three vertexes are confirmed and thereafter commences the correction process in lower/middle atmosphere. The cut-off point can be corrected by systematic uncertainties removal, therefore the correction for the initial point is imperative for following progresses (i.e., the determination of triangular-net's basic shape). The first-guess value for the initial point is derived according to previous studies (Boone et al., 2005). By considering both accuracy and efficiency, the ARTS simulation is used for the initial point exclusively, besides, iterative stride generation for the correction of the initial point is designed based on modified tangential function as follows:

$$strides = h_{min} + (h_{max} - h_{min}) \times normalize[tan(scaler + mover)] \quad (1)$$

$$scaler = \alpha \times \pi \times \left(\frac{i}{N-1} - 0.5\right), \quad (2)$$

$$mover = \sigma \times \left(\frac{\pi}{2} - \alpha \times \pi \times 0.5\right), \quad (3)$$

where h_{min} and h_{max} denote possible tangent height range (e.g., 0–20 km for most cases) for the initial point. The i and N denote the count per iteration (starts from 0) and the number of total iteration, respectively. Parameter α (0, 1) dominates the domain of value range for tangent function (i.e., the range for possible initial tangent height); σ (−1, 1) is the normalized first-guess tangent height that affects the tangent function origin of coordinates. The principle and merits of tangential stride generation approach concentrate on concerns involving the design of dynamic iteration strides, that is relatively smaller iteration strides around the first-guess and sparse strides in far-wing zones. Additionally, thread pooling strategy adopted in iteration stride generation is necessary for multi-core computation. The initial tangent height is finally determined in virtue of convolution of possible initial tangent heights with Gaussian weights.

The tangent heights are an increasing convex sequence, the domain of moving point is above the corrected initial

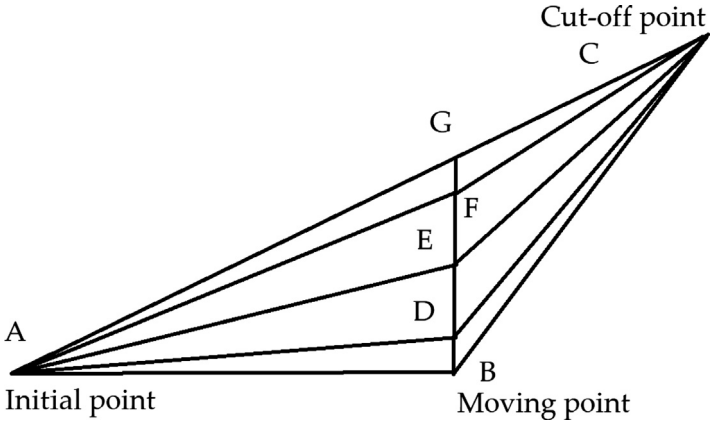

Fig. 5. The geometric structure of tangent heights correction in lower/middle atmosphere.

Please cite this article as: S. Zhu, X. Li, J. Xu et al., Neural network aided fast pointing information determination approach for occultation payloads from in-flight measurements: Algorithm design and assessment, Advances in Space Research, https://doi.org/10.1016/j.asr.2019.01.041

point (i.e., point A) and below the line connecting initial point and cut-off point (i.e., point C), vertically; for example, the possible tangent height of corrected moving point might locate in the line connecting point B and point G (e.g., point D, E or F). Iteration stride generation strategy for moving point derived from Logarithmic function is presented as follows:

$$strides = (h_{cut-off} - h_{init}) \times \log_{10} \frac{i+10}{N \times 10} \quad (4)$$

where $h_{cut-off}$ and h_{init} denote the corrected tangent height at cut-off point and the determined initial tangent height suggested by previous processes, whilst other symbols are as the same as defined in formulas above.

The construction of triangular-net is based on a series of possible tangent heights for moving point. The triangular-net is multiple groups of possible tangent height sequence for each possible moving point, and the triangular-net is achieved according to polynomial fitting while keeping the monotonicity. The tangent height series is corrected by multiple times of iteration, and each iteration is a procedure of triangular-net construction and cost calculation.

3.3. LSTM scheme

The GTI algorithm is efficiently advantageous in the lower atmosphere correction performance which is closely related to atmospheric conditions. However, in the upper atmosphere, due to stably weak absorption, a forward model is less sufficient in expression of the real atmospheric transmission simulation. Potential instrumental uncertainty, on the other hand, possibly contain biases sharing some characteristics. Long short-term memory (LSTM) is an effectively optimized network in dealing with sequential pattern recognition problems (Graves, 1997). LSTM network is an Recurrent neural network (RNN) composed of LSTM units. The basic component for a common LSTM is a memory cell. Besides, it also contains 3 gates, namely an input gate, an output gate and a forget gate. Compared to MLP (Multi-layer Perceptron), RNN is powerful in handling sequential tasks (e.g., time series), it can instantiate dynamics almost arbitrarily (Gers et al., 2014). However, standard RNNs are severely limited by the magnitude of the weights, which vary exponentially along sequences. In contrast, LSTM exhibits significant practical advantages. Due to the forget gate, the LSTM unit can dropout partial information from proceeding neurons. Therefore, it is not influenced by the gradient explosion or vanishing problems in backpropagation (Gers et al., 2014). The structure of LSTM neural network adopted in the LSTM-GTI algorithm (LSTM fine-tuning aided GTI algorithm) is depicted in Fig. 6. Here, a common LSTM unit is used; the activation function which acts as a constraint in propagation is the extensively used rectified linear unit (ReLU); the optimizer employed is Adam; the dropout rate is 0.5 and the number of batch is 200; all parameters are set as standard default values (Nair and Hinton, 2010; Kingma and Ba, 2014). Sequential record is randomly shuffled and split into 2/3 training set and 1/3 test set. In addition, the number of training epochs was set to 200.

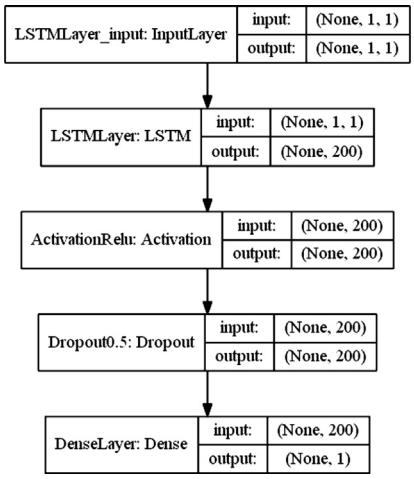

Fig. 6. LSTM neural network structure.

4. Results and discussion

4.1. GTI correction

4.1.1. Results of orbital data

Fig. 7 demonstrates the comparison of Level-1 tangent heights, ACE-FTS Level-2 tangent height products and GTI determination results. In general, the GTI algorithms shows a satisfactory performance in all 8 orbits. The Level-1 tangent heights are severely biased. The first tangent heights in 8 sequences are all far below the horizon. The largest first-point error is observed in orbit 43611, about −38.26 km from 0 km height; while the smallest in orbit 39926 with a difference about −6.94 km. Level-1 tangent heights are very linear-like, and the errors are assumed to be from systematic uncertainties and atmospheric refractivity (Boone et al., 2005). In contrasts, the Level-2 ACE products and GTI results are more like incremental quadratic curves.

Despite of the great bias in Level-1 tangent heights, the result of GTI algorithm is still in good agreement with ACE-FTS Level-2 tangent height products. The GTI shows a more satisfactory result in lower atmosphere, the difference between the corrected results and Level-2 products increased along with heights. The largest discrepancy is found universally in tangent height above 100 km, where the atmosphere is more rarefied. Because components in upper atmosphere are in low density, their influence on transmittance is more fractional, and the capability of forward model simulation is largely restricted.

4.1.2. Error analysis

The error distribution between ACE Level-2 products and GTI corrections is given in violin-plot above as shown

Please cite this article as: S. Zhu, X. Li, J. Xu et al., Neural network aided fast pointing information determination approach for occultation payloads from in-flight measurements: Algorithm design and assessment, Advances in Space Research, https://doi.org/10.1016/j.asr.2019.01.041

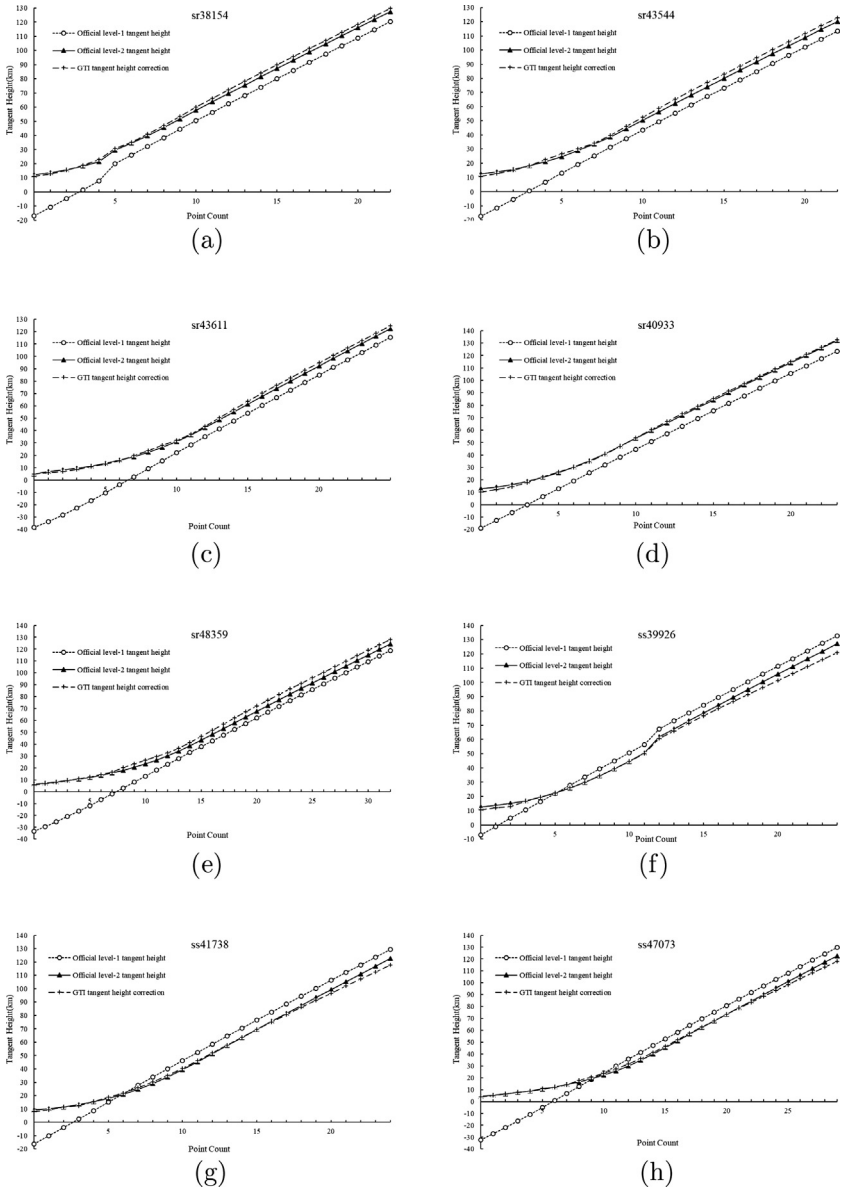

Fig. 7. Comparison between Level-1 uncorrected tangent heights, ACE-FTS corrected products and GTI algorithm results for 8 orbit data, as the title of each subplot indicates.

in Fig. 8. A violin-plot represents the distribution of one or several categorical variables, and comparison between distributions is made easily and directly. Like box-plot, but violin-plots can also demonstrate the probability density of the data at different values and plot kernel density distributions (Hullman et al., 2015).

In general, the mean discrepancy for 8 orbits is less than sensor's vertical detection resolution, i.e. 3 km. The GTI algorithm is roughly practicable in operational environment. The largest difference is found in orbit 48359 at 2.92 km and orbit 40933 is discovered with the smallest relative difference of 0.97 km. GTI algorithm is more precise in lower and middle atmosphere, because N_2 concentration is very small in upper atmosphere; for instance, the largest difference in orbit 41738 is 4.69 km at tangent point No.24, near to 120 km high. As provided in Table 3, differences in lower atmosphere in 8 orbits are all less than 1 km, expect for orbits 40933 and 39926 of 1.84 and 1.33 km, respectively. Similarly, averaged difference in middle atmosphere for 8 orbits is around 1 km, except for orbit 48359 of 2.7 km. In upper atmosphere, the difference increases up to about 2 km or larger.

Mean absolute deviation (MAD) is used to describe the statistical dispersion of the differences between the GTI corrections and ACE official Level-2 products. The MADs for 8 orbits are less than 2 km, indicating the distribution of differences is relatively dense. Among all 8 orbits, the GTI algorithm demonstrates the best determination at orbit sr40933 due to the smallest mean difference of 0.97 km and the smallest MAD of 0.9 km. Additionally,

Please cite this article as: S. Zhu, X. Li, J. Xu et al., Neural network aided fast pointing information determination approach for occultation payloads from in-flight measurements: Algorithm design and assessment, Advances in Space Research, https://doi.org/10.1016/j.asr.2019.01.041

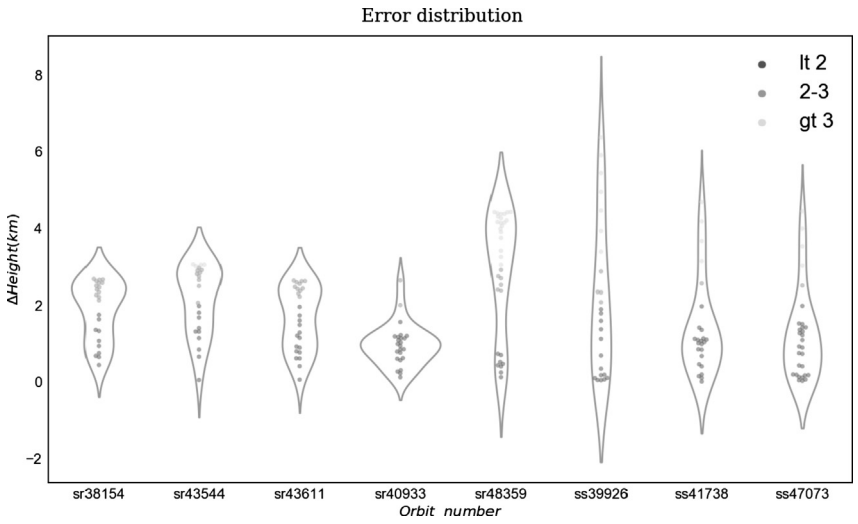

Fig. 8. Error distribution of GTI tangent height correction algorithm for 8 ACE-FTS orbits.

Table 3
Statistical indicators of error analysis for 8 orbits.

	sr38154	sr43544	sr43611	sr40933	sr48359	ss39926	ss41738	ss47073
Mean	1.86	2.12	1.64	0.97	2.92	2.14	1.41	1.23
M.A.D[a]	0.94	1.17	1.18	0.90	1.42	1.67	1.45	1.31
$Dif^{L.A.}$	0.81	0.96	0.77	1.84	0.45	1.33	0.79	0.31
$Dif^{M.A}$	1.12	1.34	1.19	0.49	2.70	0.08	1.07	1.41
$Dif^{U.A}$	2.26	2.73	2.27	0.87	4.03	3.10	1.75	1.69
R^2	0.9972	0.9959	0.9978	0.9992	0.9930	0.9935	0.9972	0.9979
PCC	0.9998	0.9997	0.9998	0.9998	0.9997	0.9996	0.9995	0.9996
p-value	1.26×10^{-37}	2.18×10^{-35}	8.29×10^{-43}	1.64×10^{-39}	2.61×10^{-51}	7.80×10^{-37}	7.00×10^{-36}	4.59×10^{-45}

[a] The mean absolute deviation.

the R^2 and Pearson correlation coefficient (PCC) which range from 0 to 1 are employed to reveal the similarity between GTI corrections and ACE official Level-2 products. The R^2 and PCC coefficients are all larger than 0.99. The p-values of PCC representing the statistical significance of similarity are all lower than 0.05, which infer the GTI algorithm is reliable in some level.

4.2. Fine-tuning with LSTM

4.2.1. Results of orbital data

As discussed above, relative differences are primarily observed in upper atmosphere. The uncertainty could be attributed to the weak absorption and low concentration of N_2 in upper. Consequently, N_2 collision induced absorption is far less sensitive. Given that, forward model is limited in accurate transmittance simulation in this vertical region, and corresponding tangent height determination approach might be not feasible here.

To increase the robustness and reliability of tangent height determination algorithm in industrial environment, the LSTM neural network was employed to facilitate the algorithm performance. As given in Fig. 9, the GTI results combined LSTM fine-tuning technique are exhibited above. Apparently, the accuracy of corrections is optimized, especially in upper atmosphere. The theoretical core of LSTM aided method is to shuffle tangent heights only of upper atmosphere. The randomly selected training and test procedure is a broadly adopted method to avoid dependency on dataset itself. Furthermore, tangent heights of middle atmosphere are the result of convolution of GTI tangent heights and the extrapolation of LSTM prediction. This modification has enhanced proposed GTI algorithm and demonstrates a relatively acceptable result in experiments on 8 ACE-FTS orbits.

4.2.2. Error analysis

Fig. 10 presents error distribution of corrections utilizing LSTM-GTI algorithm. Apparently, compared with pure GTI algorithm, the error range is largely reduced into 0–2 km for almost all orbits. Except for orbit 40933, differences between LSTM-GTI algorithm and official approach distributes more densely. The largest mean difference is 2.07 km of orbit 39926 and the smallest is 0.97 km found in orbit 38154. According to Table 4, MADs agree that the difference is reduced, and its distribution becomes more concentrated than that of pure GTI. Combining Tables 3 and 4, the largest MAD of GTI is 1.67 km at orbit 39926

Please cite this article as: S. Zhu, X. Li, J. Xu et al., Neural network aided fast pointing information determination approach for occultation payloads from in-flight measurements: Algorithm design and assessment, Advances in Space Research, https://doi.org/10.1016/j.asr.2019.01.041

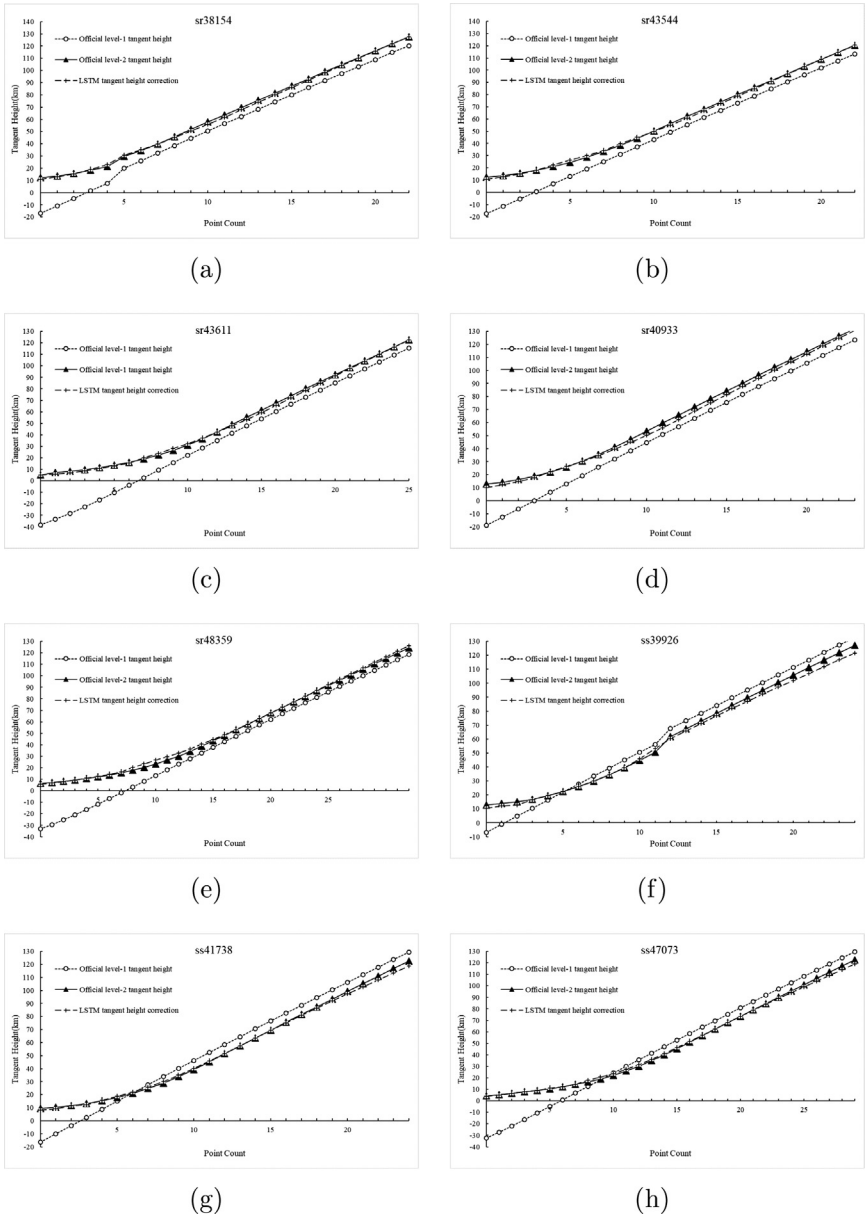

Fig. 9. Comparison between Level-1 uncorrected tangent heights, ACE-FTS corrected products and GTI algorithm adopting LSTM fine-tuning strategy results for 8 orbit data, as the title of each subplot indicates.

and it is reduced to 1.55 km by using LSTM-GTI. MADs of all orbits decrease obviously, except in orbit 40933 which increases about 0.01 km. Specifically, as suggested in Table 4, the difference declines at least 3.41% (orbit 39926) and the largest of 56.15% reduction is observed in orbit 43544. Although the overall correction is quite satisfactory in orbit 40933, the difference of LSTM-GTI increases about 107.54% compared with which of pure GTI algorithm.

Generally, R^2 coefficients of LSTM-GTI increase slightly while PCCs show a less than 0.03% decrement. Although a minor loss of statistical correlation, the LSTM-GTI exhibits an overall advantage in time consumption and an accuracy increment in layered correction.

In terms of difference in layered atmosphere, the mean difference in lower/middle atmosphere of all orbits barely show distinct change. In contrast, accuracy of tangent height determination in upper atmosphere is enhanced to a considerable extent. For most orbits, the discrepancies between LSTM-GTI results and official Level-2 products are reduced by more than a half. Admittedly, there are still some significant differences can be found after the adoption LSTM fine-tuning. Overall, these relatively large deviations are acceptable compared with ACE-FTS's vertical resolution. Additionally, the massive application of LSTM-GTI algorithm in industry must satisfy the requirements of robustness and run-time limitation, which will be discussed in following part.

Please cite this article as: S. Zhu, X. Li, J. Xu et al., Neural network aided fast pointing information determination approach for occultation payloads from in-flight measurements: Algorithm design and assessment, Advances in Space Research, https://doi.org/10.1016/j.asr.2019.01.041

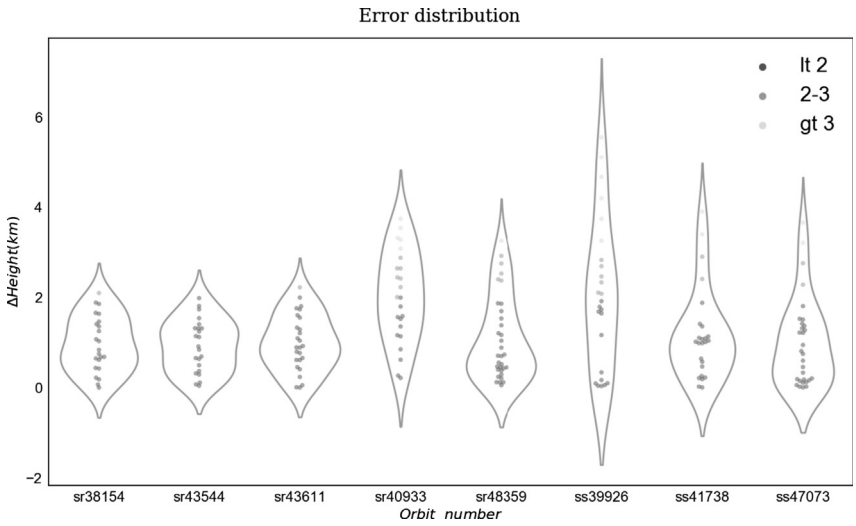

Fig. 10. Error distribution of LSTM aided GTI tangent height correction algorithm for 8 ACE-FTS orbits.

Table 4
Statistical indicators of error analysis for 8 orbits of LSTM aided GTI.

	sr38154	sr43544	sr43611	sr40933	sr48359	ss39926	ss41738	ss47073
Mean	0.97	0.93	1.00	2.01	1.09	2.07	1.17	0.99
M.A.D	0.80	0.89	0.83	0.91	0.90	1.55	1.17	1.02
$Dif^{L.A.}$	0.81	0.96	0.77	1.84	0.45	1.33	0.79	0.31
$Dif^{M.A}$	0.86	1.34	1.19	0.70	2.70	0.08	1.07	1.41
$Dif^{U.A}$	1.04	0.78	1.08	2.50	0.84	2.98	1.35	1.24
R^2	0.9990	0.9990	0.9990	0.9966	0.9986	0.9948	0.9982	0.9986
PCC	0.9996	0.9995	0.9996	0.9995	0.9996	0.9993	0.9993	0.9997
p-value	8.49×10^{-35}	1.90×10^{-33}	1.92×10^{-39}	1.83×10^{-35}	1.05×10^{-49}	7.95×10^{-35}	1.10×10^{-37}	1.31×10^{-47}
$Per.^{L.A.}$[a]	3.57%	3.84%	2.89%	7.76%	1.77%	12.61%	8.55%	3.63%
$Per.^{M.A}$	7.28%	11.69%	10.02%	7.63%	22.66%	8.51%	68.92%	85.27%
$Per.^{U.A}$	17.85%	13.26%	18.60%	41.93%	12.52%	37.64%	15.02%	13.80%
$Per.^{imp}$[b]	47.82%	56.15%	39.27%	−107.54%	62.84%	3.41%	16.84%	19.41%

[a] The percentage of (Corrected tagent heights - Level-2 products)/ (Corrected tangent heights - Level-1 tangent heights).
[b] Percentage of determination improvement by adopting LSTM fine-tuning technique.

4.3. Computaiton platform and time consumption

The GTI algorithm is designed for operational processing, therefore the maximum number of iterations is largely limited due to the time requirement. The algorithm prototype is developed in Python 2.7.12/Anaconda 4.3.14 and has been deployed on the platform with an eight-core Intel® Core™ i7-4790 CPU @ 3.60 GHz, of which the RAM is 20 GB and the Graphics processor is AMD Radeon™ R7 350.

Table 5 gives the time-consumption of tangent heights correction for three orbits. The average time for processing is about 0.27 h (i.e., 16.6 min). The cost is defined as the quadratic sum of difference between simulated and observed transmittances. In aggregate, cost at the finial iteration is relatively small. The largest cost is observed in orbit 43611 of 0.14, and this is possibly related to the limitation of iteration count and the design of algorithm. For the other orbits, the cost is less than 0.07 and it is relatively satisfactory for this algorithm. In comparison with the closed-source official algorithm, the GTI algorithm is designed for easy-to-use and time-consumption is prior to the very high accuracy. Moreover, LSTM-aided GTI algorithm was tested in 8 orbits. The total time consumed in tangent height determination of 8 orbits was 29 s, and the results as discussed above are satisfactory in industry.

Table 5
The time-consumption and quadratic sum loss of tangent correction algorithm for 8 orbital data, respectively.

Scene ID	Time-consumption	Quadratic sum loss
38154	0.32[a]	0.03[b]
43544	0.26	0.04
43611	0.25	0.14
40993	0.31	0.07
48359	0.25	0.05
39926	0.27	0.02
41738	0.28	0.06
47073	0.25	0.04

[a] The unit of time-consumption is hours.
[b] The loss is the quadratic sum of the difference transmittances of ARTs simulations and satellite-based observed transmittances.

Please cite this article as: S. Zhu, X. Li, J. Xu et al., Neural network aided fast pointing information determination approach for occultation payloads from in-flight measurements: Algorithm design and assessment, Advances in Space Research, https://doi.org/10.1016/j.asr.2019.01.041

5. Conclusions

Pointing information (tangent heights) is a crucial parameter for occultation observations to achieve reliable profile information. Here, we propose a fast, easy-to-use approach for tangent height determination in operational processing of satellite data. The approach is LSTM-aided geometrical triangular iteration (GTI) algorithm (LSTM-GTI).

Combined with comprehensive analysis in previous pointing information determination studies, the LSTM-GTI algorithm is developed in this study to meet the operational environment requirements for other occultation payloads including recently launched GF-5/AIUS. It is a geometrical algorithm with less reliance on atmospheric parameters and features triangular-net iteration. Consequently, several tricks (e.g., tangential stride generator, multi-core computation and triangular-net technique) are adopted to achieve the objectives of dynamic iteration strides and robust demands. This approach is comprised of three major processes, systematic uncertainties removal, determination of initial tangent point and triangular-net optimization. Additionally, to meet the requirements of time-consumption in industrial application, LSTM neural network is introduced to decrease determination time. Besides, it is also employed to remedy the defect of pure GTI approach due to the weak N_2 absorption in upper atmosphere.

Experiments were carried out using 8 ACE-FTS Level-1 orbital data and the results show a satisfactory performance and are in a great agreement with ACE Level-2 tangent height products (i.e., the average correlation coefficient is greater than 0.99). The average processing time is about 0.27 h with averaged cost of ~0.06 which indicates that the LSTM-GTI is a generally sound algorithm. In terms of analyses regarding errors, the average uncertainty of 8 orbits is 1.79 km and corresponding mean MAD is 1.26 km. Nevertheless, as aforementioned, the vertical detection resolution of ACE-FTS is about 3 km, thereby the correction effectiveness by employing the GTI algorithm is reasonable and the design of this approach proposed can be plausible in some levels.

The total determination time consumption is reduced to approximate 29 s for 8 orbits, and this is a significant enhancement. In addition, the average uncertainty of 8 orbits is decreased to 1.28 km with a corresponding mean MAD of 1.01 km. Compared with pure GTI algorithm, LSTM-GTI is better because the average difference of all 8 orbits is reduced by approximate 28.49%. Although the LSTM-GTI has corrected the most of errors, one remaining issue is that the deviations in the partial orbits (e.g., orbit 40933) have not been completely removed. This issue will be carefully investigated and addressed concerning extra atmospheric parameters; for instance, the co-retrieval of p/T will be integrated in the algorithm in the future. In addition, pertinent algorithm for middle and upper atmosphere will be on track as well.

Acknowledgement

This work was supported by the State Key Laboratories of Remote Sensing Science and Digital Earth Science, the General Program of National Natural Science Foundation of China (Grant No. 41571345), the Special Foundation for Free Exploration of State Laboratory of Remote Sensing Science (Grant No. Y1Y00202KZ), the National Key Research and Development Program of China (Grant No. 2018YFB050490303), and the Major Projects of High Resolution Earth Observation System (Grant No. 32-Y20A18-9001-15-17-1). The ACE-FTS data were provided by ACE-FTS team. ACE, also known as SCISAT, is a Canadian-led mission mainly supported by the Canadian Space Agency (CSA). The ARTS forward model is downloaded from the website http://www.radiativetransfer.org/.

References

Bernath, P.F., 2003. The ace (atmospheric chemistry experiment) satellite mission: An overview.

Boone, C.D., Ray, N., Walker, K.A., Yves, R., Mcleod, S.D., Rinsland, C.P., Bernath, P.F., 2005. Retrievals for the atmospheric chemistry experiment fourier-transform spectrometer. Appl. Opt. 44 (33), 7218–7231.

Buehler, S.A., Eriksson, P., Kuhn, T., Engeln, A.V., Verdes, C., 2005. Arts, the atmospheric radiative transfer simulator. J. Quantitat. Spectrosc. Radiat. Transfer 91 (1), 65–93.

Castellanos, P., Boersma, K., Torres, O., De Haan, J., 2015. Omi tropospheric NO_2 air mass factors over South America: effects of biomass burning aerosols. Atmosph. Measur. Tech. 8 (9), 3831–3849.

Chung, J.W., Lee, M.E., Kang, S.T., Bolan, N.S., 2014. Concentration distribution of carbonyl compounds in an industrial shipbuilding complex. Ksce J. Civil Eng. 18 (4), 927–932.

Cortesi, U., Bianco, S.D., Ceccherini, S., Gai, M., Dinelli, B.M., Castelli, E., Oelhaf, H., Woiwode, W., Höpfner, M., Gerber, D., 2016. Synergy between middle infrared and millimeter-wave limb sounding of atmospheric temperature and minor constituents. Atmosph. Measur. Tech. 9 (5), 2267–2289.

Dutil, Y., Poulin, R.H., 2002. ACE-FTS level 0-to-1 data processing. Proceedings of SPIE – The International Society for Optical Engineering, vol. 4814, pp. 102–110.

Eriksson, P., Buehler, S., Davis, C., Emde, C., Lemke, O., 2011. Arts, the atmospheric radiative transfer simulator, version 2. J. Quant. Spectrosc. Radiat. Transfer 112 (10), 1551–1558.

Foucher, P., Chédin, A., Dufour, G., Bernath, P., Boone, C., 2007. Feasibility of monitoring CO_2 from ACE-FTS solar occultation instrument. In: AGU Fall Meeting.

Foucher, P., Chédin, A., Dufour, G., Capelle, V., Boone, C., Bernath, P., 2008. CO_2 profile retrieval from limb viewing solar occultation made by the ACE-FTS Instrument. Agu Fall Meeting Abst. 9 (1), 2873–2890.

George, M., Clerbaux, C., Hurtmans, D., Turquety, S., Coheur, P.-F., Pommier, M., Hadji-Lazaro, J., Edwards, D., Worden, H., Luo, M., et al., 2009. Carbon monoxide distributions from the IASI/METOP mission: evaluation with other space-borne remote sensors. Atmosph. Chem. Phys. 9 (21), 8317–8330.

Gers, F.A., Schmidhuber, J., Cummins, F., 2014. Learning to forget: continual prediction with LSTM. Neural Comput. 12 (10), 2451–2471.

Graves, A., 1997. Long short-term memory. Neural Comput. 9 (8), 1735–1780.

Harrison, J., Cai, S., Dudhia, A., Chipperfield, M., Boone, C., Bernath, P., 2014. Retrievals of carbonyl fluoride (COF_2) from ACE-FTS and MIPAS spectra and their comparison with SLIMCAT CTM calculations. EGU General Assembly Conference Abstracts, vol. 16.

Please cite this article as: S. Zhu, X. Li, J. Xu et al., Neural network aided fast pointing information determination approach for occultation payloads from in-flight measurements: Algorithm design and assessment, Advances in Space Research, https://doi.org/10.1016/j.asr.2019.01.041

Hendrick, F., Roozendael, M.V., Chipperfield, M.P., Dorf, M., Goutail, F., Yang, X., Fayt, C., Hermans, C., Pfeilsticker, K., and Pommereau, J.P., 2007. Characterization of MIPAS elevation pointing.

Hullman, J., Resnick, P., Adar, E., 2015. Hypothetical outcome plots outperform error bars and violin plots for inferences about reliability of variable ordering. PloS One 10 (11), e0142444.

Höpfner, M., Emde, C., 2005. Comparison of single and multiple scattering approaches for the simulation of limb-emission observations in the mid-ir. J. Quantit. Spectrosc. Radiat. Transfer 91 (3), 275–285.

Jethva, H., Torres, O., Chen, Z., Ahn, C., et al., 2011. Comparative analysis of OMI and Aeronet retrieval of single-scattering albedo in dust and biomass burning environment. In: AGU Fall Meeting Abstracts.

Kerzenmacher, T., Wolff, M., Strong, K., Dupuy, E., Walker, K., Amekudzi, L., Batchelor, R., Bernath, P., Berthet, G., Blumenstock, T., et al., 2008. Validation of no 2 and no from the atmospheric chemistry experiment (ace). Atmospheric Chemistry and Physics 8 (19), 5801–5841.

Kingma, D.P., Ba, J., 2014. Adam: A method for stochastic optimization. arXiv preprint arXiv:1412.6980.

Lafferty, W.J., Solodov, A.M., Weber, A., Olson, W.B., Hartmann, J.M., 1996. Infrared collision-induced absorption by n(2) near 4.3 μm for atmospheric applications: measurements and empirical modeling. Appl. Opt. 35 (30), 5911.

LI, X., CHEN, L., SU, L., Zhang, Y., Tao, J., 2013. Overview of sub-millimeter limb sounding [j]. Journal of Remote Sensing 17 (6), 1325–1344.

Manney, G.L., Daffer, W.H., Strawbridge, K.B., Walker, K.A., Boone, C. D., Bernath, P.F., Kerzenmacher, T., Schwartz, M.J., Strong, K., Sica, R.J., 2008. The high arctic in extreme winters: vortex, temperature, and mls and ace-fts trace gas evolution. Atmospheric Chemistry & Physics 8 (3), 505–522.

Nair, V., Hinton, G.E., 2010. Rectified linear units improve restricted boltzmann machines. In: International Conference on International Conference on Machine Learning, pp. 807–814.

Ofipcc, W.G.I., 2013. Climate change; the physical science basis. Contribution of Working 43 (22), 866–871.

Rothman, L.S., Gordon, I.E., Babikov, Y., Barbe, A., Benner, D.C., Bernath, P.F., Birk, M., Bizzocchi, L., Boudon, V., Brown, L.R., et al., 2013. The hitran2012 molecular spectroscopic database. J. Quant. Spectrosc. Radiat. Transfer 130, 4–50.

Sandy, O., Badi-Uz-Zaman, K., Ryan, D., Evans, G.J., Mike, F., Jervis, R.E., 2004. Receptor modeling of toronto pm2.5 characterized by aerosol laser ablation mass spectrometry. Environmental Science & Technology 38 (21), 5712.

Sioris, C.E., Boone, C.D., Bernath, P.F., Zou, J., Mcelroy, C.T., Mclinden, C.A., 2010. Atmospheric chemistry experiment (ace) observations of aerosol in the upper troposphere and lower stratosphere from the kasatochi volcanic eruption. Journal of Geophysical Research Atmospheres 115 (D2).

Steck, T., Glatthor, N., Clarmann, T.v., Fischer, H., Flaud, J., Funke, B., Grabowski, U., Höpfner, M., Kellmann, S., Linden, A., et al., 2008. Retrieval of global upper tropospheric and stratospheric formaldehyde (h 2 co) distributions from high-resolution mipas-envisat spectra. Atmospheric Chemistry and Physics 8 (3), 463–470.

Suleiman, R., Chance, K., Liu, X., et al., 2013. Omi bro measurements: Operational data analysis algorithm and initial validation. In: AGU Fall Meeting Abstracts.

Terao, Y., Logan, J.A., 2005. Analysis of interannual variability in stratospheric ozone as seen by SAGE II, HALOE, SBUV(/2) and Ozonesondes, and implications for ozone trends.

Urban, J., 2014. Microwave limb sounding of the UT/LS: Stratosphere-troposphere exchange and climate monitor (STEAM) and related projects. 40th COSPAR Scientific Assembly, vol. 40.

Voulgarakis, A., Telford, P., Aghedo, A., Braesicke, P., Faluvegi, G., Abraham, N., Bowman, K., Pyle, J., Shindell, D., 2011. Global multi-year O_3-CO correlation patterns from models and TES satellite observations. Atmosph. Chem. Phys. 11 (12), 5819–5838.

Wang, Y., Beirle, S., Lampel, J., Koukouli, M., De Smedt, I., Theys, N., Ang, L., Wu, D., Xie, P., Liu, C., et al., 2017. Validation of OMI, GOME-2A and GOME-2B tropospheric NO_2, SO_2 and HCHO products using MAX-DOAS observations from 2011 to 2014 in Wuxi, China: investigation of the effects of priori profiles and aerosols on the satellite products. Atmosph. Chem. Phys. 17 (8), 5007.

Xiaoying, L.I., Chen, L., Guo, A., Lin, S.U., Jia, S., Tao, J., Ying, Z., 2015. Sub-millimeter wave limb sounding simulation of the plume flow of a high-flying vehicle. J. Remote Sens.

Zhou, X.M., Tan, J.H., Xiang, P., He, X.L., Guo, S.J., Duan, J.C., He, K. B., Ma, Y.L., Deng, S.X., Situ, S.P., 2017. Chemical characteristics of atmospheric Carbonyls in winter and summer in Foshan city. China Environ. Sci. 37 (3), 844–850.

Zhu, S., Li, X., Yu, C., Wang, H., Wang, Y., Miao, J., 2018. Spatiotemporal variations in satellite-based formaldehyde (HCHO) in the Beijing-Tianjin-Hebei region in China from 2005 to 2015. Atmosphere 9 (1), 5.

Please cite this article as: S. Zhu, X. Li, J. Xu et al., Neural network aided fast pointing information determination approach for occultation payloads from in-flight measurements: Algorithm design and assessment, Advances in Space Research, https://doi.org/10.1016/j.asr.2019.01.041